
EFFICIENT HAMILTONIAN-AWARE QUANTUM NATURAL GRADIENT DESCENT FOR VARIATIONAL QUANTUM EIGENSOLVERS

Chenyu Shi

Applied Quantum Algorithms Leiden, Leiden University
 Leiden Institute of Advanced Computer Science, Leiden University
 c.shi@liacs.leidenuniv.nl

Hao Wang

Applied Quantum Algorithms Leiden, Leiden University
 Leiden Institute of Advanced Computer Science, Leiden University
 h.wang@liacs.leidenuniv.nl

November 19, 2025

ABSTRACT

The Variational Quantum Eigensolver (VQE) is one of the most promising algorithms for current quantum devices. It employs a classical optimizer to iteratively update the parameters of a variational quantum circuit in order to search for the ground state of a given Hamiltonian. The efficacy of VQEs largely depends on the optimizer employed. Recent studies suggest that Quantum Natural Gradient Descent (QNG) can achieve faster convergence than vanilla gradient descent (VG), but at the cost of additional quantum resources to estimate Fubini-Study metric tensor in each optimization step. The Fubini-Study metric tensor used in QNG is related to the entire quantum state space and does not incorporate information about the target Hamiltonian. To take advantage of the structure of the Hamiltonian and address the limitation of additional computational cost in QNG, we propose Hamiltonian-aware Quantum Natural Gradient Descent (H-QNG). In H-QNG, we propose to use the Riemannian pullback metric induced from the lower-dimensional subspace spanned by the Hamiltonian terms onto the parameter space. We show that H-QNG inherits the desirable features of both approaches: the low quantum computational cost of VG and the reparameterization-invariance of QNG. We also validate its performance through numerical experiments on molecular Hamiltonians, showing that H-QNG achieves faster convergence to chemical accuracy while requiring fewer quantum computational resources.

1 Introduction

The Variational Quantum Eigensolver (VQE) [1] is a hybrid quantum–classical algorithm well-suited for current noisy intermediate-scale quantum devices [2]. It is a variational quantum algorithm [3] specifically designed to search for the ground state of a given Hamiltonian. VQEs have attracted wide attention across different research fields, such as quantum chemistry [4, 5], quantum many-body problems [6, 7], and materials engineering [8, 9], and is believed to hold potential for quantum advantage over classical methods [1, 10]. The basic idea of VQEs is to employ a classical optimizer to iteratively update the parameters of a parametrized quantum circuit in order to minimize the expectation value of the Hamiltonian, where the expectation value is evaluated via the output of the parameterized quantum circuit. The optimal parameters obtained by this minimization correspond to an approximate ground state of the given Hamiltonian.

Despite its promising prospects across different fields, one of the main limitations of VQEs lies in their trainability. Recent studies have shown that VQEs can suffer from serious training issues [11, 12]. Finding a suitable optimizer

is believed to be crucial for revealing the potential quantum advantages of VQEs. The basic optimization method is gradient descent, which we refer to as vanilla gradient descent in this paper. Many improved gradient-based methods have been proposed for VQEs [13–15]. Among these methods, Quantum Natural Gradient Descent (QNG) has emerged as a promising approach [15] as the quantum analog of classical natural gradient descent [16]. QNG leverages the Fubini-Study metric tensor to modify the gradient in each optimization step to capture the geometric information of quantum states.

QNG is believed to offer several advantages over vanilla gradient descent. First, like its classical counterpart, QNG is reparameterization-invariant [15, 17], whereas vanilla gradient descent generally is not. Reparameterization invariance is considered a desirable property of optimization methods, as it enhances the efficiency of the optimization process [18]. In addition, QNG is potentially helpful for avoiding local minima—one of the most significant issues affecting the trainability of VQEs [19]. Moreover, several experimental studies have shown that QNG achieves faster convergence speed than vanilla gradient descent [15, 20, 21].

However, despite its advantages, QNG requires additional quantum computational cost compared to vanilla gradient descent. In each optimization step of QNG, the Fubini-Study metric must be experimentally estimated on hardware [20, 22]. For a general parameterized circuit in VQEs with m parameters and a target Hamiltonian $H = \sum_{r=1}^v a_r P_r$ consisting of v Pauli terms, the quantum computational cost is $O(mv + m^2)$ in terms of sampling complexity for each optimization step. The mv term arises from computing the gradient with respect to each parameter, while the m^2 term corresponds to evaluating the metric tensor. By contrast, each vanilla gradient descent step only requires $O(mv)$ quantum computational cost for the gradient. Moreover, estimating the Fubini-Study metric tensor also requires additional circuits for the Hadamard test [20, 23]. This raises an interesting question: Is it possible to construct an optimization method that requires the same quantum computational cost as VG, yet achieves performance comparable to or even better than QNG?

The inspiration for our method comes from the observation that, in the general case, an n -qubit target Hamiltonian $H = \sum_{r=1}^v a_r P_r$ does not contain all 4^n Pauli strings and is therefore associated only with a non-trivial lower-dimensional subspace spanned by each term P_r . For example, a one-qubit Hamiltonian $H = -X - Y$ is independent of the z -axis, and its expectation value depends only on the coordinates in the xy -plane. Hence, H is related only to the unit disc in the xy -plane, rather than to the entire Bloch sphere. An illustration is provided in Figure 2.

Motivated by this observation, we propose considering the metric tensor used in optimization directly induced from this non-trivial lower-dimensional space. Accordingly, our method employs the Riemannian pullback metric induced from this subspace spanned by Hamiltonian terms onto the parameter space (see Definition 3), instead of using the Fubini-Study metric tensor defined over the entire quantum state space. Since the metric tensor in our method incorporates information from the target Hamiltonian, we refer to our approach as *Hamiltonian-aware Quantum Natural Gradient Descent* (H-QNG).

In this work, we show that H-QNG requires the same quantum computational cost $O(mv)$ as vanilla gradient descent. Moreover, we prove that H-QNG preserves the reparameterization-invariant property of standard QNG. Besides, by incorporating the structure of the Hamiltonian into the metric tensor, H-QNG can potentially achieve faster convergence compared to standard QNG. We experimentally display this improved convergence speed performance in this work. All experiments in this work are performed on the classical simulator, where exact quantities can be tracked noiselessly. Particularly, we also discuss the impact of shot noise through additional experiments in Section B.

The remainder of the paper is structured as follows. Section 2 briefly introduces the background knowledge required for this work. Section 3 formulates H-QNG and reveals its differences and connections to standard QNG. Section 4 analyzes the key properties of H-QNG and provides experimental application examples to display its performance. Finally, Section 5 concludes the paper.

2 Preliminaries

2.1 Variational Quantum Eigensolver

The Variational Quantum Eigensolver (VQE) [1] is a hybrid quantum–classical algorithm designed to search for the ground state ρ_G of a given target Hamiltonian H . The general workflow of VQEs is shown in Figure 1. In VQEs, a parameterized quantum circuit is used to prepare a variational state $\rho_\theta = U(\theta)|0\rangle\langle 0|U^\dagger(\theta)$ where $\theta \in \mathbb{R}^m$. Given a target Hamiltonian H , the expectation value $f(\theta) = \text{tr}(\rho_\theta H)$ is estimated on quantum devices. The ground state ρ_G is the lowest-energy state of the target Hamiltonian H . Hence, searching for ρ_G is equivalent to minimizing the expectation value function $f(\theta)$ by adjusting the tunable parameters θ .

Considering the expectation value $f(\theta)$ as the cost function, we can apply a classical optimizer to iteratively update the parameters θ , while evaluating the required quantities on the quantum device. The most common yet simple method is gradient descent (which we refer to as vanilla gradient descent in this paper to distinguish it from other gradient-based methods). In vanilla gradient descent, the parameter update rule is given by:

$$\theta^{(k+1)} = \theta^{(k)} - \eta \nabla f(\theta^{(k)}) \quad (1)$$

where $\nabla f(\theta^{(k)})$ denotes the gradient of the cost function (expectation value), and η is the learning rate. In each optimization step, the gradients are evaluated on quantum devices using techniques such as finite differences or the parameter-shift rule [24, 25]. Beyond vanilla gradient descent, many gradient-based methods have been proposed and evaluated for VQEs [14]. With a good optimizer and an expressive circuit, VQEs is expected to obtain a good approximation of the ground state ρ_G after sufficient optimization.

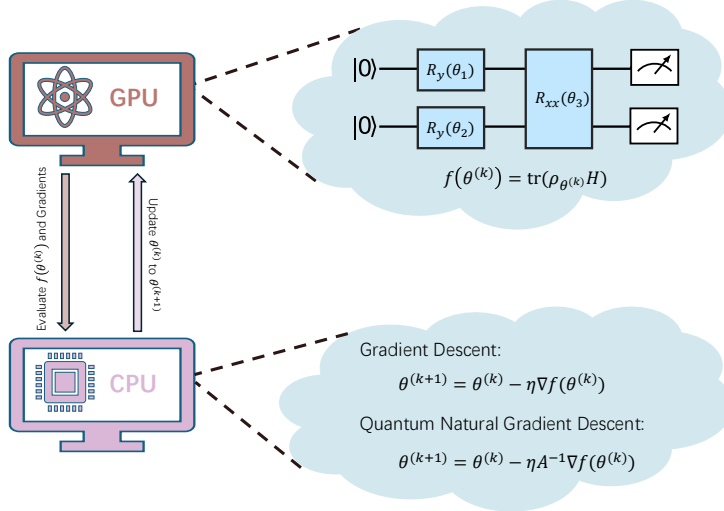


Figure 1: The general workflow of VQEs. In the quantum part, a parameterized quantum circuit is used to estimate the expectation value $\text{tr}(\rho_{\theta^{(k)}} H)$ and its gradient, given the current parameters $\theta^{(k)}$. In the classical part, a classical optimizer iteratively updates the parameters from $\theta^{(k)}$ to $\theta^{(k+1)}$ in order to minimize the expectation value. Various optimizers can be employed in the optimization of VQEs, and the choice plays an important role in its performance.

2.2 Quantum Natural Gradient Descent

In each optimization step, vanilla gradient descent solves the following constrained optimization problem [26]:

$$\begin{aligned} \min_{\delta} \quad & f(\theta + \delta) \\ \text{s.t.} \quad & \|\delta\|_2^2 \leq \varepsilon \end{aligned} \quad (2)$$

This constrained optimization problem minimizes the cost function within a local neighborhood of the current parameters $\theta^{(k)}$. In Section C, we show that the constrained optimization problem above yields the vanilla gradient descent update formula Equation (1) via a first-order Taylor approximation. One limitation of vanilla gradient descent is that each optimization step is inherently tied to the Euclidean geometry of the parameter space, since the Euclidean distance is used to define the local neighborhood in Equation (2). It has been shown that the Euclidean geometry is suboptimal for optimizing quantum variational algorithms [15, 27], and the optimization outcome may vary under different reparameterizations [15, 28]. This can lead to potential inefficiencies in the optimization of VQEs [15, 16].

Quantum natural gradient descent (QNG) [15] is a gradient-based optimization method designed for variational quantum algorithms. It is the quantum analog of natural gradient descent [16] in classical machine learning. Instead of only considering Euclidean geometry in the parameter space, QNG accounts for the quantum geometry of the state space to modify the gradient. In each optimization step, QNG solves the following contained optimization problem, where the local neighborhood is defined by fidelity distance between quantum states:

$$\begin{aligned} \min_{\delta} \quad & f(\theta + \delta) \\ \text{s.t.} \quad & D_F(\rho_\theta, \rho_{\theta+\delta}) \leq \varepsilon \end{aligned} \tag{3}$$

where the fidelity distance $D_F(\rho_\theta, \rho_{\theta+\delta}) = 1 - (\text{tr}(\sqrt{\sqrt{\rho}\sigma\sqrt{\rho}}))^2$. Similarly, Equation (3) can also yield the update rule of QNG. In Definition 1, we present the formal definition of QNG and its update rule.

Definition 1. (*Quantum Natural Gradient Descent*). *For pure variational quantum states $|\phi_\theta\rangle$ with $\theta = (\theta_1, \dots, \theta_m)^T$, the quantum natural gradient descent step with respect to the expectation value $f(\theta) = \langle\phi_\theta|H|\phi_\theta\rangle$ is defined as:*

$$\theta^{(k+1)} = \theta^{(k)} - \eta A^{-1} \nabla f(\theta^{(k)}) \tag{4}$$

where $A_{ij} = \text{Re}[\langle\partial_i\phi_\theta|\partial_j\phi_\theta\rangle - \langle\partial_i\phi_\theta|\phi_\theta\rangle\langle\phi_\theta|\partial_j\phi_\theta\rangle]$ is the Fubini-Study metric tensor.

The derivation from Equation (3) to Equation (4) is shown in Section C. As we can see, the Fubini-Study metric tensor is used to modify the gradient in each optimization step. To address the limitation of vanilla gradient descent, QNG takes into account the geometry of the quantum state, and it is reparameterization-invariant [15]. Several experimental studies further indicate that QNG achieves faster convergence speed than vanilla gradient descent [15, 20, 21].

Despite its many advantages, a main limitation of QNG is the requirement of additional quantum computational costs. As shown in Equation (4), the Fubini-Study metric tensor is required in each optimization step. In the general case, this metric tensor is not available in analytic form and must be estimated empirically on hardware [29]. To address this limitation, we propose a method that avoids additional quantum computational costs.

3 Method Formulation

In this section, we formally present the proposed method in Definition 3. Before introducing our definition, we first review the notion of the pullback metric [30–32] and explain how it can be used to perform gradient-based optimization in Definition 2. We also show that QNG, as defined in Definition 1, can be interpreted from the perspective of the pullback metric in Proposition 1. Detailed proofs for the results in this section are provided in Section D. We also reveal the connections and differences between our method and the related work OP-VQITE [33] in Section A.

Definition 2. (*Pullback Metric*). *Consider an immersion $h : \mathcal{S} \rightarrow \mathcal{M}$ from a parameter space \mathcal{S} to a Riemannian Manifold \mathcal{M} equipped with a Riemannian metric $G_{\mathcal{M}}$. A pullback metric G_θ on \mathcal{S} is induced by the immersion h . For $\theta \in \mathcal{S}$ and $u, v \in \mathcal{T}_\theta \mathcal{S}$, G_θ is given by:*

$$G_\theta(u, v) = G_{\mathcal{M}}(dh_\theta(u), dh_\theta(v)) \tag{5}$$

Particularly, if \mathcal{S} and \mathcal{M} are both Euclidean space with coordinates, then the matrix form of the pullback metric is given by:

$$G = J_h^T J_h \tag{6}$$

where J_h is the Jacobian of h at θ . Hence, the element of the matrix $G_{ij} = \langle\partial_i h(\theta), \partial_j h(\theta)\rangle$.

A detailed discussion of above definition of the pullback metric can be found in [30]. The Riemannian pullback metric can be used to define a gradient-based optimization [31] with respect to a cost function $f = g \circ h : \mathcal{S} \rightarrow \mathbb{R}$ where $h : \mathcal{S} \rightarrow \mathcal{M}$ and $g : \mathcal{M} \rightarrow \mathbb{R}$. For each $\theta \in \mathcal{S}$, the gradient descent with the pullback metric is defined as:

$$\theta^{(k+1)} = \theta^{(k)} - \eta G^{-1} \nabla f(\theta^{(k)}) \tag{7}$$

where G is the matrix form of the pullback metric defined in Definition 2. Here, we show that the QNG defined in Definition 1 can be interpreted from the perspective of the gradient descent with Riemannian pullback metric in Proposition 1.

Proposition 1. *For an n -qubit VQE, suppose parameter space $\mathcal{S} \in \mathbb{R}^m$, and let $\mathcal{M} \subseteq \mathbb{R}^{4^n}$ be the image of the space of $2^n \times 2^n$ Hermitian matrices under the mapping: $Q \rightarrow [\text{tr}(QP_1), \dots, \text{tr}(QP_{4^n})]$, where Q is an arbitrary $2^n \times 2^n$ Hermitian matrix and P_r ($1 \leq r \leq 4^n$) are the possible Pauli strings. The metric $G_{\mathcal{M}}$ is the Euclidean Riemannian metric in \mathbb{R}^{4^n} . The gradient descent with Riemannian pullback metric for the cost function $f(\theta) = \text{tr}(\rho_\theta H)$ can be formulated as Equation (7), where the pullback metric G is equal to Fubini-Study metric tensor A up to a factor: $G = 2^{n+1} A$.*

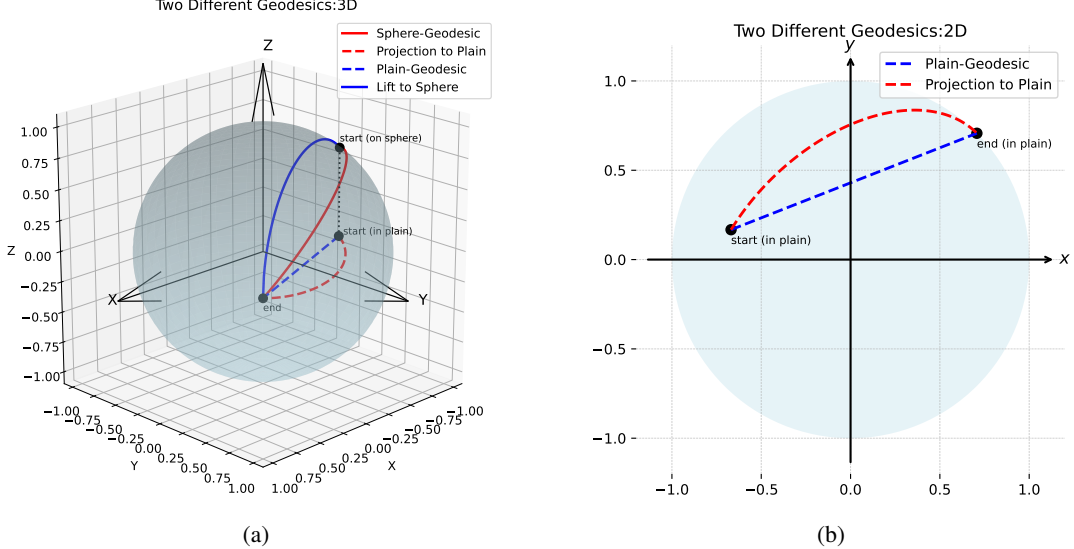


Figure 2: To minimize the expectation value of the Hamiltonian $H = -X - Y$, only the manifold embedded in lower dimensional space (the unit disc with boundary in (b)) contributes non-trivially to the optimization rather than the entire Bloch sphere (the sphere in (a)), since the z -axis coordinate does not appear in the cost function. The geodesic with respect to the spherical metric (red solid line in (a)) represents the shortest path on the Bloch sphere from the initial point to the solution. However, its projection onto the non-trivial xy -plain (red dotted lines in a and b) is not the shortest path compared to the true geodesic within the xy -plain (blue dotted lines in a and b). Therefore, in the pullback metric view, H-QNG directly employs $g_{\mathcal{M}}$ as the metric of the non-trivial manifold in Definition 3, in contrast to standard QNG which considers $g_{\mathcal{M}}$ to be the metric of the full quantum state space in Proposition 1.

Proposition 1 shows that the Riemannian pullback metric differs from the Fubini-Study metric tensor in QNG only by a constant factor. Since the constant factor c can be absorbed into the learning rate, QNG defined in Definition 1 is fully equivalent to the gradient descent with Riemannian pullback metric in Proposition 1.

The function $h : \mathcal{S} \rightarrow \mathcal{M}$ in Proposition 1 maps a parameter $\theta \in R^m$ to the vector $[\text{tr}(\rho_{\theta} P_1), \dots, \text{tr}(\rho_{\theta} P_{4^n})] \in R^{4^n}$, and the corresponding function $g : \mathcal{M} \rightarrow \mathbb{R}$ is a linear combination of these 4^n elements such that $g \circ h(\theta) = f(\theta) = \text{tr}(\rho_{\theta} H)$. However, the target Hamiltonian $H = \sum_r a_r P_r$ typically involves only a subset of the 4^n Pauli operators in general. Therefore, we can restrict the function h to include only the relevant v terms and discard the others. In other words, the cost function $f(\theta)$ is only determined by a manifold embedded in the lower dimensional space $\mathcal{M} \subseteq \mathbb{R}^v$. A one-qubit example is shown in Figure 2. The manifold \mathcal{M} here represents the Bloch sphere. However, for the Hamiltonian $H = -X - Y$, only the 2-dimensional manifold (a unit disc with boundary) in XY -plain contributes to the optimization since the objective function does not contain any component in the z -axis direction. Moreover, since the coefficients of the linear combination are determined by the Hamiltonian, they can be directly incorporated into the function h as well, which rescales the lower-dimensional manifold. Based on this observation, we define a new gradient descent method with Riemannian pullback metric directly on the non-trivial manifold as the proposed method of this paper in Definition 3. We name it as *Hamiltonian-aware Quantum Natural Gradient Descent* (H-QNG), to distinguish it from the standard QNG, where the Fubini-Study metric is not related to the given Hamiltonian.

Definition 3. (Hamiltonian-aware Quantum Natural Gradient Descent (H-QNG)). For an n -qubit VQE with Hamiltonian $H = \sum_{r=1}^v a_r P_r$, suppose parameter space $\mathcal{S} \in \mathbb{R}^m$, and let $\mathcal{M} \in \mathbb{R}^{4^n}$ be the image of the space of $2^n \times 2^n$ Hermitian matrices under the mapping: $Q \rightarrow [a_1 \text{tr}(Q P_1), \dots, a_v \text{tr}(Q P_v)]$, where Q is an arbitrary $2^n \times 2^n$ Hermitian matrix and P_r ($1 \leq r \leq v$) are the Pauli strings in the Hamiltonian H . The metric $g_{\mathcal{M}}$ is the Euclidean Riemannian metric in \mathbb{R}^v . The gradient descent with Riemannian pullback metric for the cost function $f(\theta) = \text{tr}(\rho_{\theta} H)$ can be formulated as Equation (7), where the pullback metric $G_{ij} = \sum_r a_r^2 \text{tr}(\partial_i \rho_{\theta} P_r) \text{tr}(\partial_j \rho_{\theta} P_r)$. The Hamiltonian-aware Quantum Natural Gradient Descent is defined as:

$$\theta^{(k+1)} = \theta^{(k)} - \eta T^{-1} \nabla f(\theta^{(k)}) \quad (8)$$

where $T_{ij} = \frac{1}{2\sqrt{\sum_{r=1}^v a_r^2}} G_{ij}$. When $v = 4^n$ and each $a_r = 1$, H-QNG reduces to standard QNG.

The prefactor $\frac{1}{2\sqrt{\sum_{r=1}^v a_r^2}}$ is introduced to ensure that the definition of H-QNG remains consistent with standard QNG: when $v = 4^n$ and each $a_r = 1$, the manifold in Definition 3 reduces to the manifold in Proposition 1, in which case we expect that H-QNG reduces to standard QNG. To realize this consistency, the prefactor must equal $2^{-(n+1)}$ in this condition according to Proposition 1. Hence, the prefactor $\frac{1}{2\sqrt{\sum_{r=1}^v a_r^2}}$ is used to appropriately scale G_{ij} .

As shown in Equation (4), the metric tensor G does not require additional quantum measurement cost, as each gradient term in its expression is already required for evaluating $\nabla f(\theta)$. In contrast, the standard QNG demands extra quantum resources to compute the Hilbert–Schmidt metric tensor. The detailed analysis about computational cost scaling will be discussed in Section 4.1.

One desired properties of standard QNG is its invariance under diffeomorphism reparameterization [15, 20]. That is, the optimization of standard QNG remains unchanged under diffeomorphism transformations of the parameter space. This reparameterization invariance is believed to improve the optimization process, which is discussed in [18]. In Section 4.2, we show and prove that H-QNG also possesses this property.

We note that the definition of the pullback metric in Definition 2 requires the function h to be an immersion. However, the map $h : \theta \in \mathbb{R}^m \rightarrow [a_1 \text{tr}(\rho_\theta P_1), \dots, a_v \text{tr}(\rho_\theta P_v)] \in \mathbb{R}^v$ realized by a variational quantum circuit, is not always guaranteed to be an immersion. This may affect the condition number and the invertibility of the resulting matrix G of H-QNG. In Section 4.3, we show that the matrix G is almost everywhere invertible in the typical application scenario of VQEs. We also introduce regularization methods to address cases where G is non-invertible or ill-conditioned.

4 Method Analysis

4.1 Scaling Analysis

In this subsection, we analyze the quantum computational costs of H-QNG. We do not consider classical computational costs in this subsection, such as the inversion of the metric tensor.

Firstly, we analyze the quantum measurement overhead of each optimization step, which is proportional to the number of quantities that required to be estimated during each optimization step. Here we assume an equal number of measurement shots per quantity estimation. For the quantum measurement overhead of vanilla gradient descent and QNG, we present the following proposition.

Proposition 2. *For an n -qubit VQE with m parameters and a given Hamiltonian $H = \sum_{r=1}^v a_r P_r$ consisting of v terms, the quantum measurement overheads of each optimization step of vanilla gradient descent and QNG are $O(mv)$ and $O(mv + m^2)$, respectively.*

Proof. For vanilla gradient descent, each optimization step requires evaluating the gradient with respect to each parameter for each Hamiltonian term $\partial_{\theta_i} \text{tr}(\rho_\theta P_r)$, using the parameter-shift rule [34, 35]. Since each partial derivative requires to estimate two quantities using parameter-shift rule, the total number of measurement overhead per optimization step is proportional to $2mv$ ^{*}. For QNG, in addition to the gradient, each optimization step requires estimating the Fubini-Study metric tensor, which is an $m \times m$ matrix. Because it is symmetric, there are approximately $\frac{m^2}{2}$ elements to be estimated. Each element can be evaluated using Hadamard test [20, 23], which involves four quantity estimations via the parameter-shift rule. As a result, the total number of circuit estimations per optimization step of QNG is $O(mv + m^2)$. \square

As shown in Proposition 2, each optimization step of QNG requires higher quantum measurement overhead compared to vanilla gradient descent. For H-QNG, we now present the following theorem regarding its quantum computational complexity.

Theorem 1. *For an n -qubit VQE with m parameters and a given Hamiltonian $H = \sum_{r=1}^v a_r P_r$ consisting of v terms, the quantum measurement overhead of each optimization step of H-QNG is $O(mv)$.*

Proof. Note that computing each element of the matrix T in Equation (8) only requires all the partial derivative terms, which have already been estimated during the gradient estimation. Therefore, estimating the matrix T in H-QNG does not require any additional quantum measurement overhead, and the total cost remains $O(mv)$. \square

Proposition 2 and Theorem 1 show that H-QNG requires the same quantum measurement overhead as vanilla gradient descent. Compared to standard QNG, each optimization step of H-QNG is more efficient in terms of quantum

^{*}Here we suppose each pair of Pauli terms contained in the Hamiltonian is non-commutative in general.

resource usage. Besides, H-QNG can even achieve a better convergence speed compared to standard QNG in terms of optimization step. We conduct a numerical experiment to illustrate this result in Figure 3.

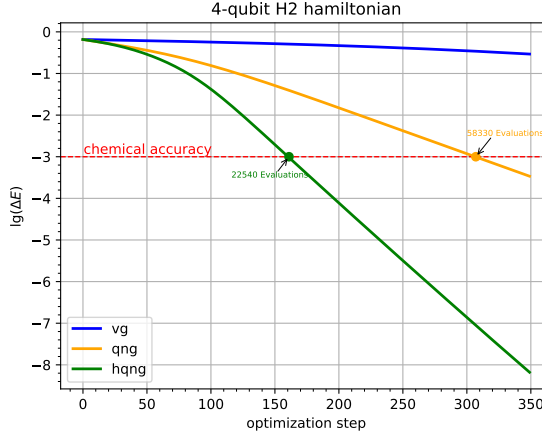


Figure 3: The energy distance from the ground state ΔE of a 4-qubit H_2 Hamiltonian using vanilla gradient descent (blue line), QNG (orange line), and H-QNG (green line). All three methods start from the identical initial parameters. H-QNG reaches chemical accuracy (red dotted line) earlier than standard QNG, both in terms of optimization steps and quantum circuit evaluations (in the unit of quantity to be estimated). Both standard QNG and H-QNG significantly outperform vanilla gradient descent.

Figure 3 shows the energy distance from the ground state for a 4-qubit H_2 Hamiltonian using vanilla gradient descent, standard QNG, and H-QNG. The Hamiltonian used in the experiment contains 15 terms (including identity), the specific formulation of the Hamiltonian and variational circuit are from the PennyLane Molecules library [36]. All three methods start from the identical initial parameters. In terms of optimization steps (horizontal axis), H-QNG (green line) reaches chemical accuracy (red dotted line) faster than standard QNG (orange line). We also report the number of circuit evaluations required to achieve chemical accuracy in the unit of quantity to be estimated, using conclusion from Proposition 2 and Theorem 1. Since each optimization step of H-QNG requires fewer quantum measurement overheads, it reaches chemical accuracy even faster in terms of total circuit evaluations compared to standard QNG. Besides, we notice that vanilla gradient descent fails to achieve chemical accuracy within the given optimization budget. As H-QNG and vanilla gradient descent have the same measurement overhead, H-QNG significantly outperforms vanilla gradient descent in convergence speed under the same quantum computational budget.

In addition to measurement overhead, compared to standard QNG, H-QNG also requires lower circuit complexity. As discussed in Proposition 2, estimating elements of the Fubini-Study metric tensor requires techniques such as the Hadamard test or swap test, which involve additional ancillary qubits or deeper quantum circuits. In contrast, H-QNG introduces no additional circuit complexity.

4.2 Reparameterization Invariance

One of the most important properties of standard QNG is the invariance under reparameterization given by a diffeomorphism [15, 20]. Here we give a brief definition to the reparameterization invariance property for an optimization method in Definition 4.

Definition 4. (Reparameterization Invariance for an Optimization Method). *Consider a reparameterization given by a diffeomorphism $\theta = t(\psi)$. Suppose in a step of the optimization, the parameter θ is updated to θ' , and correspondingly ψ is updated to ψ' . An optimization method is said to be reparameterization invariant if, whenever $\theta = t(\psi)$, it holds that $\theta' = t(\psi')$ after the update.*

To discuss the reparameterization invariance property of QNG and H-QNG, we express both methods in the form of differential equations, which we refer to as the continuous form of QNG and H-QNG.

$$\dot{\theta}(t) = -A_\theta^{-1} \nabla_\theta f(\theta) \quad (9)$$

$$\dot{\theta}(t) = -T_\theta^{-1} \nabla_\theta f(\theta) \quad (10)$$

Equation (9) and Equation (10) lead to Equation (4) and Equation (8), respectively, through the finite difference method [37]. In practical use, with a sufficiently small learning rate and an adequate number of optimization steps, Equation (4) and Equation (8) can be regarded as good discrete approximations of Equation (9) and Equation (10), respectively. We specifically refer to Equation (9) and Equation (10) as the continuous forms of QNG and H-QNG, to distinguish them from their usual discrete forms in Equation (4) and Equation (8). Based on these formulations, we further establish Proposition 3 and Theorem 2.

Proposition 3. *Continuous form of Quantum Natural Gradient Descent defined in Equation (9) is reparameterization invariant.*

The property in Proposition 3 has been discussed in [15, 20]. In Theorem 2, we demonstrate that H-QNG also possesses reparameterization invariance. The detailed proof of Theorem 2 is provided in Section E.

Theorem 2. *Continuous form of Hamiltonian-aware Quantum Natural Gradient Descent defined in Equation (10) is reparameterization invariant.*

Theorem 2 and Definition 4 indicates that, just as in standard QNG, given any initial point $\theta^{(0)} = t(\psi^{(0)})$, H-QNG will follow two equivalent trajectories $\{\theta^{(k)}\}$ and $\{\psi^{(k)}\}$ in these two parameter spaces, where each $\theta^{(k)} = t(\psi^{(k)})$. Besides, note that Proposition 3 and Theorem 2 assume that these gradient-based methods are in the continuous form, but in practice only a finite number of steps can be taken. With a small learning rate, QNG taking finite steps is approximately parameterization invariant [17]. For H-QNG, a similar conclusion can be drawn as in [17] for QNG.

We also evaluate this property through numerical experiments where H-QNG can only take finite steps with small learning rates. The results are shown in Figure 4. Three different reparameterization functions t are used. The optimization is performed in the ψ -space for obtain the trajectories $\{\psi^{(k)}\}$, with the same initial point in the θ -space where $\theta^{(0)} = t(\psi^{(0)})$. The reparameterization invariance ensures that the trajectories $\{\theta^{(k)}\}$ in the θ -space obtained by $t(\{\psi^{(k)}\})$ remain unchanged regardless of different choices of t . As shown in the figures, the trajectories plotted in θ -space remain invariant under different reparametrizations for both QNG and H-QNG (the blue curve and red curve). However, this invariance does not hold for vanilla gradient descent (the cyan curve).

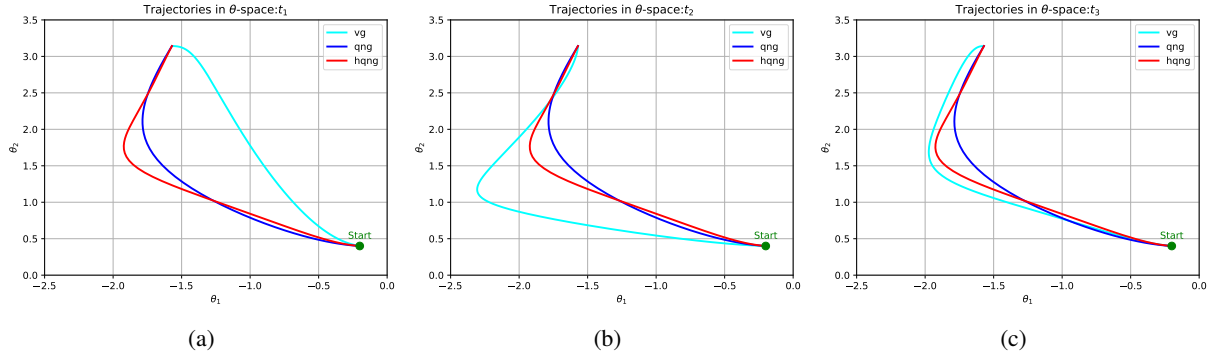


Figure 4: Evaluating the reparameterization invariant property for vanilla gradient descent, QNG and H-QNG. The given 2-qubit Hamiltonian is $H = X_1 + Y_1 + Z_1 + X_2 + Y_2 + Z_2 + X_1 X_2 + Y_1 Y_2 + Z_1 Z_2$. The experiments are performed using a 2-parameter VQE circuit composed of Pauli rotation and CNOT gates, evaluated under three optimization methods. The cost function is given by $\text{tr}(\rho(\theta_1, \theta_2)H)$, where the optimal solution can be analytically obtained as $\theta_1 = -\frac{\pi}{2}$ and $\theta_2 = \pi$. Optimization is carried out using three different reparameterization functions t in the ψ -space where $t_1 : (\theta_1, \theta_2) = (0.8\psi_1, 1.2\psi_2)$, $t_2 : (\theta_1, \theta_2) = (1.2\psi_1, 0.8\psi_2)$, $t_3 : (\theta_1, \theta_2) = (2 \arctan(2 \tan(0.5\psi_1)), 2 \arctan(2 \tan(0.5\psi_2)))$. The initial points $\psi^{(0)}$ in ψ -space are chosen such that they correspond to the same point in θ -space under each mapping t . The trajectories $\{\theta^{(k)}\}$ are obtained by applying each t to the corresponding trajectories in the ψ -space. The trajectories of QNG and H-QNG remain invariant in the θ -space (the blue curve and red curve), whereas this invariance does not hold for vanilla gradient descent (the cyan curve).

4.3 Singularity of the Metric Tensor

Definition 2 requires the function h to be an immersion; otherwise, the pullback metric may be singular. However, this immersion condition does not always hold for variational quantum circuits, where different parameter values may result in the same variational quantum state. In this section, we prove that, in general, the metric tensor T used in H-QNG is almost everywhere non-singular in the parameter space. We begin by formulating the following proposition for standard QNG. The detailed proofs of propositions and theorems in this subsection are shown in Section F.

Proposition 4. For an n -qubit VQE with m parameters and a given Hamiltonian $H = \sum_{r=1}^v a_r P_r$, the Fubini-Study metric tensor A used in QNG can only be either:

1. Almost everywhere non-singular for θ in the parameter space.
2. Everywhere singular for θ in the parameter space.

In the general case of a well-constructed parameterization, the Fubini-Study metric tensor should not be constantly singular. Under this condition, Proposition 4 implies that singularities of the Fubini-Study metric tensor can only occur in a small subspace of measure zero within the entire parameter space. This property guarantees that the standard QNG remains well-defined at almost all points in the parameter space. We also aim for H-QNG to preserve this desirable property. Fortunately, as shown in the following theorem, this is indeed the case for H-QNG.

Theorem 3. For an n -qubit VQE with m parameters and a given Hamiltonian $H = \sum_{r=1}^v a_r P_r$, the metric tensor T used in H-QNG can only be either:

1. Almost everywhere non-singular for θ in the parameter space.
2. Everywhere singular for θ in the parameter space.

The specific singularity property that the metric tensor T follows among the two possible ones in Theorem 3 depends on the relative magnitudes of m and v , namely the number of parameters in the ansatz and the number of Pauli terms in the Hamiltonian. For the case $m > v$, the function h fails to be an immersion, and the metric tensor T is everywhere singular for θ in the parameter space. However, the condition $m > v$ is not typical for the application of VQEs on NISQ devices. NISQ quantum devices limit VQEs to shallow quantum circuits [2, 38], where the number of parameters can only grow moderately with the number of qubits n , such as $O(n \text{ polylog } n)$ [20]. In contrast, the number of terms in the Hamiltonian can grow much faster, such as $O(n^4)$ for molecular systems in quantum chemistry [20, 39]. This typically ensures that $m < v$ in typical applications of VQEs such as quantum chemistry.

In the more general case where $m < v$, the metric tensor T used in H-QNG is non-singular almost everywhere in the parameter space under a good parameterization. This property implies that the metric tensor T is well-defined throughout most of the parameter space, similarly to the case of standard QNG.

However, Proposition 4 and Theorem 3 only ensure that the metric tensors are non-singular in most regions of the parameter space; they do not guarantee a good condition number. Moreover, the optimization trajectory may still pass through singular points, such as in the case of frustration-free Hamiltonians [40], where the optimal point is singular. For instance, standard QNG uses the Moore–Penrose inverse of the Fubini-Study metric tensor instead of its exact inverse, as proposed in the original paper [15]. Alternatively, the regularization can also be adopted by adding a scaled identity matrix, i.e. $A + \lambda I$, where λ is a tunable hyperparameter. For H-QNG, we adopt the latter method since it is more widely used in recent researches [20, 26, 36, 41–43]. The choice of λ is crucial and requires careful tuning, as illustrated in Figure 5. The other experimental setting is the same as that in Figure 3. From the results, we can see that a value of λ that is too large can lead to slow convergence, while a value that is too small may fail to adequately regularize the metric tensor, potentially causing oscillations, non-convergence, or early convergence. General strategies for selecting λ are discussed in [44].

4.4 Application Examples

In this section, we evaluate H-QNG against standard QNG and vanilla gradient descent (VG) as baseline methods on two molecular Hamiltonian examples: the 12-qubit LiH Hamiltonian and the 12-qubit H_6 Hamiltonian. The formulations of the Hamiltonians and the variational circuits used for training are both from the PennyLane Molecules Library [36]. In this formulation, the solution that can achieve chemical accuracy is guaranteed to lie within the search space of the variational circuit. The initial parameters are randomly generated around the optimal solutions provided by PennyLane to evaluate the local convergence properties of all methods. The regularization factor λ is set as 0.1 for H-QNG. We report the achieved energy E , and the energy distance ΔE from the ground-state energy on a logarithmic scale, both averaged over 10 independent runs.

From Figure 6 and Figure 7, we observe that H-QNG achieves competitive performance compared to standard QNG for both Hamiltonians, and it even reaches chemical accuracy faster than standard QNG in terms of optimization steps. Moreover, since each optimization step of H-QNG requires fewer shots than standard QNG, it achieves chemical accuracy with even lower overall computational cost. In addition, we note that both H-QNG and standard QNG significantly outperform vanilla gradient descent, which fails to achieve chemical accuracy within the given budget of 100 optimization steps.

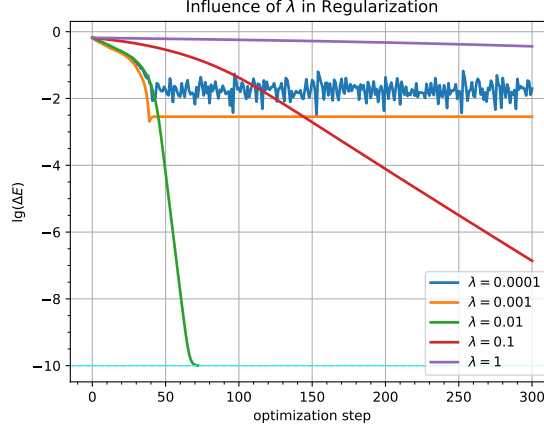


Figure 5: The influence of λ in regularization for H-QNG. The experiment records the energy distance from the ground state ΔE of a 4-qubit H_2 Hamiltonian using different values of the regularization hyperparameter λ in H-QNG. The learning curves are plotted until a precision of 10^{-10} (cyan line). A large value of λ leads to slow convergence (purple line), while a small λ may result in oscillations (blue line) or early convergence (orange line).

These results highlight the potential advantage of H-QNG: it requires the same quantum computational cost as vanilla gradient descent, while achieving performance that is even superior to standard QNG. We speculate that this performance improvement arises from the observation that the physically relevant states occupy only a small subspace of the full Hilbert space [45, 46]. This may further suggest that, for ground-state optimization problems, focusing on the optimization in the nontrivial manifold spanned by the target Hamiltonian terms could be more effective than considering the entire quantum state space. In addition, another possible reason for H-QNG’s superior performance is that it explicitly incorporates the coefficients of the Hamiltonian terms, which helps the optimizer better weight the step size along different directions for each parameter in the optimization step.

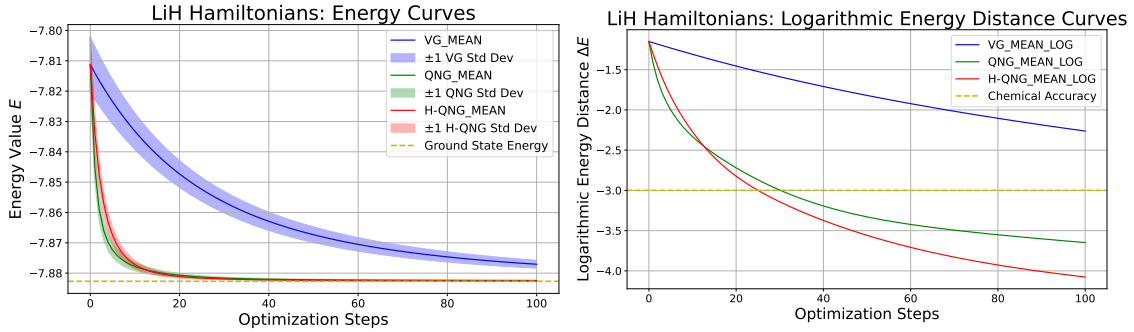


Figure 6: The energy curves (left) and the energy distance curves in logarithmic (right) over 10 independent runs for LiH Hamiltonian.

5 Conclusions and Future Works

In this work, we propose a new optimization method for the Variational Quantum Eigensolver (VQE). Our method is derived from the perspective of a Riemannian pullback metric defined on a manifold that contributes non-trivially to the cost function. Compared to standard QNG, the proposed method takes advantages of the information about the Hamiltonian when computing the metric tensor at each optimization step. The most notable advantage of H-QNG is that it only requires the same quantum computational cost as vanilla gradient descent while achieving comparable or even superior performance to standard QNG. Furthermore, we prove that H-QNG preserves key properties of standard QNG, such as reparameterization invariance.

Our experimental results show that H-QNG not only achieves a faster convergence speed but also requires fewer quantum computational resources. In particular, H-QNG reaches chemical accuracy more quickly than standard QNG for three different molecular Hamiltonians: H_2 , LiH, and H_6 . These results indicate the potential advantages of

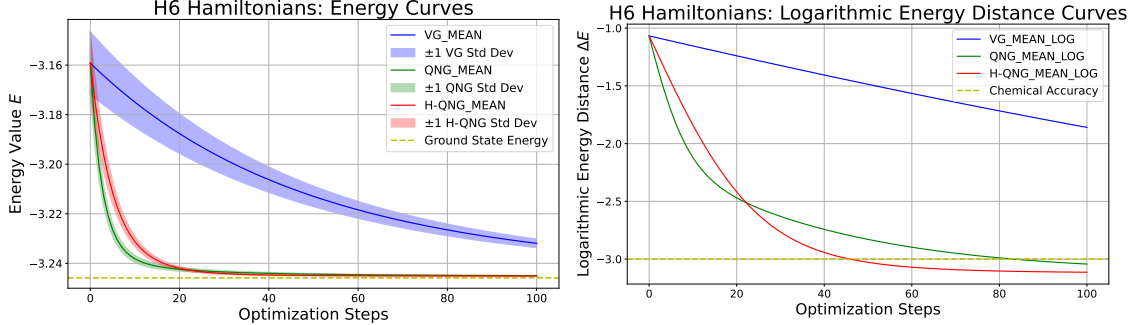


Figure 7: The energy curves (left) and the energy distance curves in logarithmic (right) over 10 independent runs for H_6 Hamiltonian.

employing H-QNG for the optimization of VQEs. We speculate that this advantage arises from H-QNG’s incorporation of information from the Hamiltonian—specifically, the optimization process is considered directly on the non-trivial manifold spanned by Hamiltonian terms, and the Hamiltonian coefficients are also used to weight the step size along each optimization direction.

In this work, we formulate H-QNG on idealized variational quantum circuits, where the required quantities can be evaluated noiselessly. We have also discussed the influence of shot noise in Section B. However, on NISQ devices, circuit noise can also affect the optimization process. Reference [20] extends standard QNG to the case with circuit noise by employing the Hilbert–Schmidt metric tensor for mixed states instead of the Fubini–Study metric tensor for pure states. For our method, the formulation in Definition 3 and the optimization update in Equation (8) can similarly be extended to mixed states and remain well defined as that in [20]. However, the performance of H-QNG under circuit noise remains to be evaluated.

This work primarily focuses on optimization for VQEs. However, we note that standard QNG can also be applied to other variational quantum algorithms, such as the variational quantum classifier in the field of quantum machine learning. Therefore, H-QNG is also expected to be applicable to problems beyond VQEs, as long as the cost function is defined via the expectation value of a given Hamiltonian. In such cases, our method is expected to provide similar advantages over standard QNG for the same reasons in VQEs. We consider evaluating the performance of H-QNG on other variational quantum algorithms as a future work.

In conclusion, H-QNG provides a promising and efficient optimization method for VQEs. By considering the manifold that contributes non-trivially to the cost function, H-QNG leverages information from the target Hamiltonian, reduces quantum computational costs, and offers a potential research direction for the optimization of variational quantum algorithms.

Acknowledgement

C.S. and H.W. thank Vedran Dunjko for insightful discussions. C.S. acknowledges the support from the European Union (ERC CoG, BeMAIQuantum, 101124342). This project was also co-funded by the Dutch National Growth Fund (NGF), as part of the Quantum Delta NL programme.

Appendix

A Comparison with OP-VQITE

Operator-Projected Variational Quantum Imaginary Time Evolution (OP-VQITE) [33] improves the standard Variational Quantum Imaginary Time Evolution (VQITE) [41] by operator projection. For a given Hamiltonian H , OP-VQITE formulates the metric tensor G and gradient term b as:

$$G_{ij} = \sum_{O \in S_\tau} \text{tr}(\partial_i \rho_\theta O) \text{tr}(\partial_j \rho_\theta O) \quad (11)$$

$$b = \sum_{O \in S_\tau} V(\rho_\theta, O) \nabla_\theta \text{tr}(\rho_\theta O) \quad (12)$$

where $V(\rho_\theta, O) = \text{tr}(\rho_\theta \{O, H\}) - 2\text{tr}(\rho_\theta H) \text{tr}(\rho_\theta O)$ and S_τ is an operator set that spans the Hamiltonian H . The corresponding parameter update rule is then formulated as:

$$\theta^{(k+1)} = \theta^{(k)} - \eta G^{-1} b \quad (13)$$

There can be a plenty of choices of the operator set S_τ . In general, H-QNG and OP-VQITE differ both in the metric tensor and in the gradient term. In a special case, for a Hamiltonian $H = \sum_{r=1}^v a_r P_r$, if the operator set is chosen as $S_\tau = \{a_r P_r \mid 1 \leq r \leq v\}$, then the metric tensor G defined in Equation (11) for OP-VQITE becomes equivalent to the metric tensor T defined in Definition 3 up to a constant prefactor. However, this equivalence of metric tensors still does not render H-QNG equivalent to OP-VQITE, because their gradient terms differ: the vector b defined in Equation (12) for OP-VQITE is not the gradient of the cost function. Since OP-VQITE requires estimating the extra expectation value terms in $V(\rho_\theta, O)$, whereas H-QNG only requires the same estimates as vanilla gradient descent, H-QNG generally has lower shot complexity than OP-VQITE. This is a potential advantage of H-QNG over OP-VQITE.

B Impact of Shot Noises

In this work, we mainly consider the ideal case where the circuit is noiseless and the required gradients and metric tensors can be precisely tracked. However, due to NISQ devices, noise can be a great matter for the optimization performance. In our case, a natural follow-up question related to noise is whether the impact of shot noise could become a serious issue for H-QNG, due to the fewer shots used in H-QNG, where both the gradient and the metric tensor are estimated using the same measurement samples. In this section, we conduct additional experiments to show that the influence of shot noise on H-QNG is not worse than that on standard QNG. Moreover, H-QNG still displays its fast convergence advantage in reaching the desired accuracy.

The experimental setup is the same as that in Section 4.1 for the H_2 Hamiltonian, except that we now include shot noise. Each element used to compute the gradient and the metric tensor is estimated using 1024 measurement shots instead of being tracked precisely. Remark that, because standard QNG requires estimating more elements than H-QNG, each optimization step of QNG consequently involves more measurement shots in total. The optimization step budget is increased to 800 for standard QNG to better display the convergence behavior of it. The learning curves are shown in Figure 8. The cost function values for plotting learning curves are still obtained exactly, in order to better analyze the impact of shot noise on the optimization process itself.

As shown in the figure, the learning curve of H-QNG with shot noise (orange line) still reaches chemical accuracy faster than standard QNG with shot noise (green line). Moreover, H-QNG with shot noise performs almost identically to the noiseless case (blue line) in the early stages, where the energy gap to the target state is large, but eventually reaches an accuracy floor due to shot noise. A similar accuracy floor also appears for standard QNG, even though it uses more measurement shots in total. These results indicate that shot noise does affect the optimization process; however, with a sufficient number of measurement shots, both methods are only mildly affected before achieving desired accuracy. In addition, H-QNG continues to display an advantage in convergence speed compared to QNG under shot noise.

C Proofs in Section 2

Here we provide a detailed derivation from the constrained optimization problem to the update formulas for vanilla gradient descent and QNG. For vanilla gradient descent, using the method of Lagrange multipliers, the constrained optimization problem given in Equation (2) can be formulated as:

$$\delta^* = \underset{\delta}{\operatorname{argmin}} f(\theta + \delta) + \lambda(\|\delta\|_2^2 - \epsilon) \quad (14)$$

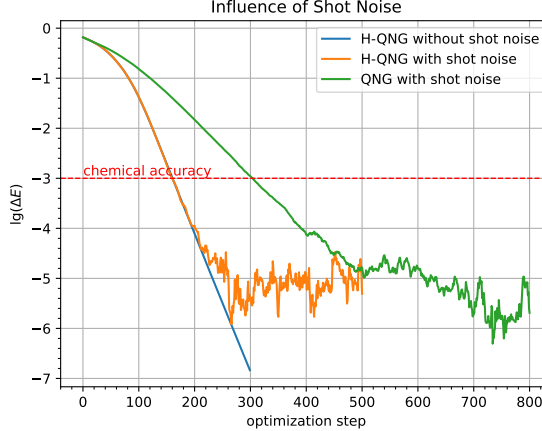


Figure 8: The learning curves of H-QNG (orange line) and QNG (green line) under shot noise, with 1024 measurement shots used for each required quantity. H-QNG still reaches chemical accuracy faster than standard QNG in the presence of shot noise. H-QNG behaves similarly to the noiseless case in the early stages but eventually encounters a precision floor due to shot noise. The same precision floor is also observed for standard QNG.

By applying the first-order Taylor expansion to $f(\theta + \delta)$, we obtain:

$$\delta^* \approx \underset{\delta}{\operatorname{argmin}} f(\theta) + \nabla f(\theta)^T \delta + \lambda(\|\delta\|_2^2 - \epsilon) \quad (15)$$

Since we are searching the minimum, Equation (15) should satisfy the Karush–Kuhn–Tucker (KKT) conditions. Here, this simply means that the derivative of the right-hand side with respect to δ must be zero:

$$\begin{aligned} 0 &= \nabla f(\theta) + 2\lambda\delta^* \\ \delta^* &= -\frac{1}{2\lambda}\nabla f(\theta) \end{aligned} \quad (16)$$

By considering $\frac{1}{2\lambda}$ as the learning rate η , we derive the exact update rule of vanilla gradient descent in Equation (1).

For QNG, the derivation proceeds in a similar way. The constrained optimization problem in Equation (3) can be formulated as:

$$\delta^* = \underset{\delta}{\operatorname{argmin}} f(\theta + \delta) + \lambda(D_F(\rho_\theta, \rho_{\theta+\delta}) - \epsilon) \quad (17)$$

Note that for pure states, we have $D_F(\rho_\theta, \rho_{\theta+\delta}) = \frac{1}{2}\|\rho_{\theta+\delta} - \rho_\theta\|_2^2$. By applying first-order Taylor expansion to $\rho_{\theta+\delta}$, we have $\rho_{\theta+\delta} \approx \rho_\theta + \sum_i \partial_i \rho_\theta \delta_i$. Hence, we have $D_F(\rho_\theta, \rho_{\theta+\delta}) \approx \frac{1}{2}\|\sum_i \partial_i \rho_\theta \delta_i\|_2^2 = \frac{1}{2}\sum_{ij} \operatorname{tr}(\partial_i \rho_\theta \partial_j \rho_\theta) \delta_i \delta_j = \delta^T A \delta$, where the matrix $A_{ij} = \frac{1}{2}\operatorname{tr}(\partial_i \rho_\theta \partial_j \rho_\theta)$ is equivalent to the Fubini–Study metric tensor when the state ρ_θ is pure [20, 26]. Substituting this expression into Equation (17) and applying the first-order Taylor expansion to $f(\theta + \delta)$, we obtain:

$$\delta^* \approx \underset{\delta}{\operatorname{argmin}} f(\theta) + \nabla f(\theta)^T \delta + \lambda(\delta^T A \delta - \epsilon) \quad (18)$$

Similarly, by applying KKT-conditions, we obtain:

$$\begin{aligned} 0 &= \nabla f(\theta) + 2\lambda A \delta^* \\ \delta^* &= -\frac{1}{2\lambda} A^{-1} \nabla f(\theta) \end{aligned} \quad (19)$$

By considering $\frac{1}{2\lambda}$ as the learning rate η , we derive the exact update rule of QNG in Definition 1.

D Proofs in Section 3

Here we provide a proof of Proposition 1. The function $h : \mathcal{S} \rightarrow \mathcal{M}$ in Proposition 1 maps a parameter $\theta \in R^m$ to a vector $[\operatorname{tr}(\rho_\theta P_1), \dots, \operatorname{tr}(\rho_\theta P_{4^n})] \in R^{4^n}$, and the corresponding function $g : \mathcal{M} \rightarrow \mathbb{R}$ is a linear combination of these

4^n elements such that $g \circ h(\theta) = f(\theta) = \text{tr}(\rho_\theta H)$. The main objective is to show that the pullback metric G defined in Proposition 1 is equal to the Fubini-Study metric tensor A up to a constant factor 2^{n+1} : $G = 2^{n+1}A$. According to Definition 2, we have:

$$\begin{aligned}
G_{ij} &= \langle [\text{tr}(\partial_i \rho P_1), \dots, \text{tr}(\partial_i P_{4^n})], [\text{tr}(\partial_j \rho P_1), \dots, \text{tr}(\partial_j P_{4^n})] \rangle \\
&= \sum_{r=1}^{4^n} \text{tr}(\partial_i \rho P_r) \text{tr}(\partial_j \rho P_r) \\
&= 2^n \text{tr}((\partial_i \rho \otimes \partial_j \rho) S) \\
&= 2^n \text{tr}(\partial_i \rho \partial_j \rho) \\
&= 2^{n+1} A_{ij}
\end{aligned} \tag{20}$$

The second equality follows from the fact that G_M is the Euclidean Riemannian metric. The third equality results from the Pauli decomposition of the swap operator. The fourth equality applies the swap trick [47]. The final equality uses the relation between the Hilbert-Schmidt metric tensor T and the Fubini-Study metric tensor A , namely $T_{ij} = 2A_{ij}$ [20,26].

Following the same derivation approach as in Equation (20), we can obtain the expression for the pullback metric G of H-QNG defined in Definition 3, where $G_{ij} = \sum_r a_r^2 \text{tr}(\partial_i \rho_\theta P_r) \text{tr}(\partial_j \rho_\theta P_r)$.

E Proofs in Section 4.2

Here we provide a brief proof of Theorem 2. Proposition 3 can be proved in a similar way. To prove Theorem 2, we introduce the following Lemma 1 for ODEs.

Lemma 1. *For two ODEs $\dot{\theta} = A(\theta)$ and $\dot{\psi} = B(\psi)$ and a diffeomorphism reparameterization h between θ and ψ where $\theta(0) = h(\psi(0))$, if for any $\theta = h(\psi)$ it holds that $A(\theta) = J_h(\psi)B(\psi)$ where $J_h(\psi)$ is the Jacobian of h at ψ , then $\theta(t) = h(\psi(t))$ for all $t \geq 0$.*

Proof. Define $F(t) = \theta(t) - h(\psi(t))$, the derivative of F with respect to t is given by $\dot{F}(t) = \dot{\theta} - J_h(\psi)\dot{\psi}$. Substituting the two ODEs into this expression yields $\dot{F}(t) = A(\theta) - J_h(\psi)B(\psi) = 0$. Since $\theta(0) = h(\psi(0))$, we have $F(0) = 0$. By the uniqueness of the solution to the ODE, it follows that $F(t) = 0$ for all $t \geq 0$, i.e., $\theta(t) = h(\psi(t))$ for all $t \geq 0$. \square

According to Lemma 1, to prove Theorem 2, we only need to prove that, for any $\theta = h(\psi)$, it holds that $T_\theta^{-1} \nabla_\theta f = J_h(\psi) T_\psi^{-1} \nabla_\psi f$. Here we introduce Lemma 2.

Lemma 2. *The cost function f and metric tensor T of H-QNG are defined by Definition 3. For a diffeomorphism reparameterization function h between θ and ψ , when $\theta = h(\psi)$, then we have $\nabla_\psi f = J_h^T(\psi) \nabla_\theta f$ and $T_\psi = J_h^T(\psi) T_\theta J_h(\psi)$.*

Proof. Suppose $\theta, \psi \in \mathbb{R}^m$. We use Einstein summation notation [48] in the derivation. For the first equation to prove, viewing the gradient as $m \times 1$ matrix for notation convenience, we have:

$$\begin{aligned}
[\nabla_\psi f]_{i1} &= \frac{\partial f}{\partial \psi_i} \\
&= \frac{\partial f}{\partial \theta_j} \frac{\partial \theta_j}{\partial \psi_i} \\
&= [J_h]^{ji} \frac{\partial f}{\partial \theta_j} \\
&= [J_h^T]^{ij} [\nabla_\theta f]_{j1}
\end{aligned}$$

The above equation is equivalent to $\nabla_\psi f = J_h^T(\psi) \nabla_\theta f$. For the second equation to prove, we have:

$$\begin{aligned}
[T_\psi]_{ij} &= \frac{1}{2\sqrt{\sum_{r=1}^v a_r^2}} \sum_{r=1}^v a_r^2 \text{tr}\left(\frac{\partial \rho}{\partial \psi_i} P_v\right) \text{tr}\left(\frac{\partial \rho}{\partial \psi_j} P_v\right) \\
&= \frac{1}{2\sqrt{\sum_{r=1}^v a_r^2}} \sum_{r=1}^v a_r^2 \text{tr}\left(\frac{\partial \rho}{\partial \theta_k} \frac{\partial \theta_k}{\partial \psi_i} P_v\right) \text{tr}\left(\frac{\partial \rho}{\partial \theta_l} \frac{\partial \theta_l}{\partial \psi_j} P_v\right) \\
&= \frac{1}{2\sqrt{\sum_{r=1}^v a_r^2}} \sum_{r=1}^v a_r^2 \text{tr}([J_h]^{ki} \frac{\partial \theta_k}{\partial \psi_i} P_v) \text{tr}([J_h]^{lj} \frac{\partial \theta_l}{\partial \psi_j} P_v) \\
&= [J^T]^{ik} [T_\theta]_{kl} [J]^{lj}
\end{aligned}$$

The above equation is equivalent to $T_\psi = J_h^T(\psi) T_\theta J_h(\psi)$. \square

Now we can prove $T_\theta^{-1} \nabla_\theta f = J_h(\psi) T_\psi^{-1} \nabla_\psi f$ from the LHS:

$$T_\theta^{-1} \nabla_\theta f = (J_h^{-T}(\psi) T_\psi J_h^{-1}(\psi))^{-1} J_h^{-T}(\psi) \nabla_\psi f \quad (21)$$

$$= J_h(\psi) T_\psi^{-1} \nabla_\psi f \quad (22)$$

The first equation follows from Lemma 2. Now, with this equation and Lemma 1, the parameterization invariance of H-QNG is proven. The parameterization invariance of standard QNG can be proven in a similar way.

F Proofs in Section 4.3

We begin by introducing the following lemma, which will be used in the proof presented in this section.

Lemma 3. *Let $H(\theta)$ be a real analytic function on $U \subseteq \mathbb{R}^m$. If H is not identically zero, then its zero set $Z(H) := \{\theta \in U : F(\theta) = 0\}$ has a zero measure, namely $\text{mes}_d Z(H) = 0$.*

The proof and discussion of Lemma 3 can be found in [49]. Therefore, to establish Proposition 4 and Theorem 3, it suffices to show that $\det(A(\theta))$ and $\det(T(\theta))$ are real analytic functions. According to [20, 23], each expectation value $h(\theta) = \text{tr}(\rho_\theta P)$ with a Pauli string P forms a trigonometric series. For a circuit of finite depth and width, this series is a finite linear combination of trigonometric functions, and hence is analytic. The determinant of the metric tensor, $T_{ij} = \frac{1}{2\sqrt{\sum_{r=1}^v a_r^2}} \sum_{r=1}^v a_r^2 \text{tr}(\partial_i \rho_\theta P_v) \text{tr}(\partial_j \rho_\theta P_v)$, is also a finite combination of such analytic functions, and is therefore itself analytic.

Therefore, according to Lemma 3, the zero set $\det(T(\theta)) = 0$ must have measure zero in the parameter space (corresponding to the second case in Theorem 3), unless the determinant is constantly zero (corresponding to the first case in Theorem 3). The proof of Proposition 4 follows by the same argument.

References

- [1] Alberto Peruzzo, Jarrod McClean, Peter Shadbolt, Man-Hong Yung, Xiao-Qi Zhou, Peter J Love, Alán Aspuru-Guzik, and Jeremy L O’brien. A variational eigenvalue solver on a photonic quantum processor. *Nature communications*, 5(1):4213, 2014.
- [2] John Preskill. Quantum computing in the nisq era and beyond. *Quantum*, 2:79, 2018.
- [3] Marco Cerezo, Andrew Arrasmith, Ryan Babbush, Simon C Benjamin, Suguru Endo, Keisuke Fujii, Jarrod R McClean, Kosuke Mitarai, Xiao Yuan, Lukasz Cincio, et al. Variational quantum algorithms. *Nature Reviews Physics*, 3(9):625–644, 2021.
- [4] Hocheol Lim, Doo Hyung Kang, Jeonghoon Kim, Aidan Pellow-Jarman, Shane McFarthing, Rowan Pellow-Jarman, Hyeon-Nae Jeon, Byungdu Oh, June-Koo Kevin Rhee, and Kyoung Tai No. Fragment molecular orbital-based variational quantum eigensolver for quantum chemistry in the age of quantum computing. *Scientific reports*, 14(1):2422, 2024.

- [5] Gleydson Fernandes de Jesus, Erico Souza Teixeira, Lucas Queiroz Galvão, Maria Heloísa Fraga da Silva, Mauro Queiroz Nooblath Neto, Bruno Oziel Fernandez, Amanda Marques de Lima, Eivson Darlivam Rodrigues de Aguiar Silva, and Clebson dos Santos Cruz. Evaluating variational quantum eigensolver approaches for simplified models of molecular systems: A case study on protocatechuic acid. *Molecules*, 30(1):119, 2024.
- [6] Gaurav Gyawali and Michael J Lawler. Adaptive variational preparation of the fermi-hubbard eigenstates. *Physical Review A*, 105(1):012413, 2022.
- [7] Tim Weaving, Alexis Ralli, Vinul Wimalaweera, Peter J Love, and Peter V Coveney. Simulating the antiferromagnetic heisenberg model on a spin-frustrated kagome lattice with the contextual subspace variational quantum eigensolver. *arXiv preprint arXiv:2506.12391*, 2025.
- [8] Tanvi P Gujarati, Mario Motta, Triet Nguyen Friedhoff, Julia E Rice, Nam Nguyen, Panagiotis KI Barkoutsos, Richard J Thompson, Tyler Smith, Marna Kagele, Mark Brei, et al. Quantum computation of reactions on surfaces using local embedding. *npj Quantum Information*, 9(1):88, 2023.
- [9] Benchen Huang, Marco Govoni, and Giulia Galli. Simulating the electronic structure of spin defects on quantum computers. *PRX Quantum*, 3(1):010339, 2022.
- [10] Abhinav Kandala, Antonio Mezzacapo, Kristan Temme, Maika Takita, Markus Brink, Jerry M Chow, and Jay M Gambetta. Hardware-efficient variational quantum eigensolver for small molecules and quantum magnets. *nature*, 549(7671):242–246, 2017.
- [11] Jarrod R McClean, Sergio Boixo, Vadim N Smelyanskiy, Ryan Babbush, and Hartmut Neven. Barren plateaus in quantum neural network training landscapes. *Nature communications*, 9(1):4812, 2018.
- [12] Martin Larocca, Supanut Thanasilp, Samson Wang, Kunal Sharma, Jacob Biamonte, Patrick J Coles, Lukasz Cincio, Jarrod R McClean, Zoë Holmes, and Marco Cerezo. Barren plateaus in variational quantum computing. *Nature Reviews Physics*, pages 1–16, 2025.
- [13] Ryan Sweke, Johannes Jakob Meyer, Paul K Fährmann, Barthélémy Meynard-Piganeau, and Jens Eisert. Stochastic gradient descent for hybrid quantum-classical optimization. *Quantum*, 4, 2020.
- [14] Benjamin DM Jones, Lana Mineh, and Ashley Montanaro. Benchmarking a wide range of optimisers for solving the fermi-hubbard model using the variational quantum eigensolver. *Quantum Science and Technology*, 10(4):045032, 2025.
- [15] James Stokes, Josh Izaac, Nathan Killoran, and Giuseppe Carleo. Quantum natural gradient. *Quantum*, 4:269, 2020.
- [16] Shun-Ichi Amari. Natural gradient works efficiently in learning. *Neural computation*, 10(2):251–276, 1998.
- [17] James Martens. New insights and perspectives on the natural gradient method. *Journal of Machine Learning Research*, 21(146):1–76, 2020.
- [18] Yang Song, Jiaming Song, and Stefano Ermon. Accelerating natural gradient with higher-order invariance. In *International Conference on Machine Learning*, pages 4713–4722. PMLR, 2018.
- [19] David Wierichs, Christian Gogolin, and Michael Kastoryano. Avoiding local minima in variational quantum eigensolvers with the natural gradient optimizer. *Physical Review Research*, 2(4):043246, 2020.
- [20] Bálint Koczor and Simon C Benjamin. Quantum natural gradient generalized to noisy and nonunitary circuits. *Physical Review A*, 106(6):062416, 2022.
- [21] Naoki Yamamoto. On the natural gradient for variational quantum eigensolver. *arXiv preprint arXiv:1909.05074*, 2019.
- [22] Tobias Haug and MS Kim. Natural parametrized quantum circuit. *Physical Review A*, 106(5):052611, 2022.
- [23] Bálint Koczor and Simon C Benjamin. Quantum analytic descent. *Physical Review Research*, 4(2):023017, 2022.
- [24] Kosuke Mitarai, Makoto Negoro, Masahiro Kitagawa, and Keisuke Fujii. Quantum circuit learning. *Physical Review A*, 98(3):032309, 2018.
- [25] Maria Schuld, Ville Bergholm, Christian Gogolin, Josh Izaac, and Nathan Killoran. Evaluating analytic gradients on quantum hardware. *Physical Review A*, 99(3):032331, 2019.
- [26] Chenyu Shi, Vedran Dunjko, and Hao Wang. Weighted approximate quantum natural gradient for variational quantum eigensolver. *arXiv preprint arXiv:2504.04932*, 2025.
- [27] Aram W Harrow and John C Napp. Low-depth gradient measurements can improve convergence in variational hybrid quantum-classical algorithms. *Physical Review Letters*, 126(14):140502, 2021.

- [28] Julien Gacon, Christa Zoufal, Giuseppe Carleo, and Stefan Woerner. Simultaneous perturbation stochastic approximation of the quantum fisher information. *Quantum*, 5:567, 2021.
- [29] André J Ferreira-Martins, Renato Farias, Giancarlo Camilo, Thiago O Maciel, Allan Tosta, Ruge Lin, Abdulla Alhajri, Tobias Haug, and Leandro Aolita. Variational quantum algorithms with exact geodesic transport. *arXiv preprint arXiv:2506.17395*, 2025.
- [30] Luis Augenstein, Noémie Jaquier, Tamim Asfour, and Leonel Rozo. On probabilistic pullback metrics on latent hyperbolic manifolds. *arXiv preprint arXiv:2410.20850*, 2024.
- [31] Qinxun Bai, Steven Rosenberg, and Wei Xu. A geometric understanding of natural gradient. *arXiv preprint arXiv:2202.06232*, 2022.
- [32] Willem Diepeveen, Georgios Batzolis, Zakhar Shumaylov, and Carola-Bibiane Schönlieb. Score-based pullback riemannian geometry. *arXiv preprint arXiv:2410.01950*, 2024.
- [33] Aeishah Ameera Anuar, François Jamet, Fabio Gironella, Fedor Simkovic IV, and Riccardo Rossi. Operator-projected variational quantum imaginary time evolution. *arXiv preprint arXiv:2409.12018*, 2024.
- [34] David Wierichs, Josh Izaac, Cody Wang, and Cedric Yen-Yu Lin. General parameter-shift rules for quantum gradients. *Quantum*, 6:677, 2022.
- [35] Stefan H Sack, Raimel A Medina, Alexios A Michailidis, Richard Kueng, and Maksym Serbyn. Avoiding barren plateaus using classical shadows. *PRX Quantum*, 3(2):020365, 2022.
- [36] Ville Bergholm, Josh Izaac, Maria Schuld, Christian Gogolin, Shahnawaz Ahmed, Vishnu Ajith, M Sohaib Alam, Guillermo Alonso-Linaje, B AkashNarayanan, Ali Asadi, et al. PennyLane: Automatic differentiation of hybrid quantum-classical computations. *arXiv preprint arXiv:1811.04968*, 2018.
- [37] Pei-bai Zhou. *Numerical analysis of electromagnetic fields*. Springer Science & Business Media, 2012.
- [38] Jonathan Wei Zhong Lau, Kian Hwee Lim, Harshank Shrotriya, and Leong Chuan Kwek. Nisq computing: where are we and where do we go? *AAPPS bulletin*, 32(1):27, 2022.
- [39] Ryota Kojima, Masahiko Kamoshita, and Keita Kanno. Orbital-rotated fermi-hubbard model as a benchmarking problem for quantum chemistry with the exact solution. *arXiv preprint arXiv:2402.11869*, 2024.
- [40] Or Sattath, Siddhardh C Morampudi, Chris R Laumann, and Roderich Moessner. When a local hamiltonian must be frustration-free. *Proceedings of the National Academy of Sciences*, 113(23):6433–6437, 2016.
- [41] Mario Motta, Chong Sun, Adrian TK Tan, Matthew J O’Rourke, Erika Ye, Austin J Minnich, Fernando GSL Brandao, and Garnet Kin-Lic Chan. Determining eigenstates and thermal states on a quantum computer using quantum imaginary time evolution. *Nature Physics*, 16(2):205–210, 2020.
- [42] Barnaby van Straaten and Bálint Koczor. Measurement cost of metric-aware variational quantum algorithms. *PRX Quantum*, 2(3):030324, 2021.
- [43] Mourad Halla. Quantum natural gradient with geodesic corrections for small shallow quantum circuits. *Physica Scripta*, 100(5):055121, 2025.
- [44] Jorge Nocedal and Stephen J Wright. *Numerical optimization*. Springer, 1999.
- [45] David Poulin, Angie Qarry, Rolando Somma, and Frank Verstraete. Quantum simulation of time-dependent hamiltonians<? format?> and the convenient illusion of hilbert space. *Physical review letters*, 106(17):170501, 2011.
- [46] Sam McArdle, Tyson Jones, Suguru Endo, Ying Li, Simon C Benjamin, and Xiao Yuan. Variational ansatz-based quantum simulation of imaginary time evolution. *npj Quantum Information*, 5(1):75, 2019.
- [47] Antonio Anna Mele. Introduction to haar measure tools in quantum information: A beginner’s tutorial. *Quantum*, 8:1340, 2024.
- [48] Alan H Barr. The einstein summation notation. *An Introduction to Physically Based Modeling (Course Notes 19)*, pages E, 1:57, 1991.
- [49] Boris Mityagin. The zero set of a real analytic function. *arXiv preprint arXiv:1512.07276*, 2015.